Journal of Alloys and Compounds 509 (2011) 7537–7542

Contents lists available at ScienceDirect

Journal of Alloys and Compounds

journal homepage: www.elsevier.com/locate/jallcom

Blue and green emissions with high color purity from nanocrystalline $Ca_2Gd_8Si_6O_{26}$:Ln (Ln = Tm or Er) phosphors

G. Seeta Rama Raju[a], Jin Young Park[a], Hong Chae Jung[a], E. Pavitra[a], Byung Kee Moon[a,*], Jung Hyun Jeong[a], Jae Su Yu[b], Jung Hwan Kim[c], Haeyoung Choi[c]

[a] Department of Physics, Pukyong National University, Busan 608-737, Republic of Korea
[b] Department of Electronics and Radio Engineering, Kyung Hee University, 1 Seocheon-dong, Giheung-gu, Yongin-si, Gyeonggi-do 446-701, Republic of Korea
[c] Department of Physics, Dong Eui University, Busan 614-714, Republic of Korea

ARTICLE INFO

Article history:
Received 13 February 2011
Received in revised form 21 April 2011
Accepted 22 April 2011
Available online 30 April 2011

Keywords:
Nanocrystalline $Ca_2Gd_8Si_6O_{26}$
Solvothermal synthesis
Photoluminescence
Cathodoluminescence
High color purity blue and green emissions

ABSTRACT

Blue and green light emissive nanocrystalline $Ca_2Gd_8Si_6O_{26}$ (CGS):Tm^{3+} and CGS:Er^{3+} phosphors with high color purity were prepared by solvothermal reaction method. The structural and morphological properties of these phosphors were evaluated by the powder X-ray diffraction (XRD) and scanning electron microscopy, respectively. From the XRD results, Tm^{3+}:CGS and Er^{3+}:CGS phosphors had the characteristic peaks of oxyapatite in the hexagonal lattice structure. The visible luminescence properties of phosphors were obtained by ultraviolet (UV) or near-UV light and low voltage electron beam (0.5–5 kV) excitation. The photoluminescence and cathodoluminescence properties were investigated by changing the variation of Tm^{3+} or Er^{3+} concentrations and the acceleration voltage, respectively. The CGS:Tm^{3+} phosphors exhibited the blue emission due to $^1D_2 \rightarrow {}^3F_4$ transition, while the CGS:Er^{3+} phosphors showed the green emission due to $^4S_{3/2} \rightarrow {}^4I_{15/2}$ transition. The color purity and chromaticity coordinates of the fabricated phosphors are comparable to or better than those of standard phosphors for lighting or imaging devices.

1. Introduction

In recent years, solid-state lighting using light emitting diodes (LEDs) and flat panel technologies such the field emission display (FED) have attracted worldwide attention because of their important benefits including energy saving, safety, reliability, maintenance and environmentally friendly characteristics [1–4]. Although the phosphor selection for fluorescent lamps, LEDs and FEDs has been made long ago there is still considerable research activity to improve the chemical stability and to adopt the materials to the production technology for the respective applications [3–6]. Luminescent materials with very high stability, which is invariable to operating conditions, is required for ongoing miniaturization, working lifetime improvement and spectral stability of fluorescent lamps on the one hand and brightness/contrast improvement in imaging systems on the other hand. Among the imaging devices, FEDs are attracting significant interest as one of the most promising FPD technologies because they have many advantages such as thin panel thickness, self emission, distortion-free image, wide viewing angle and quick response, as well as low power consumption [2,7–9]. A serious problem with the development of full color FEDs is the lack of suitable blue and green luminescent materials with high luminescence, good chromaticity, and superior color quality at low electron beam excitation ($\leq$5 kV) [8,10,11]. Sulfide-based compounds such as ZnS:Ag [12] for blue and Gd_2O_2S:Tb^{3+} [11] for green have been explored as possible phosphors for FEDs. However, the instability of sulfur has prohibited their use in the FEDs. The conventional sulfide-based phosphors often degrade under high energy electron bombardment due to the cation-sulfur bond dissociation. The process produces corrosive sulfur-bearing gas species that contaminate emission tips and reduce device lifetime. Blue oxide phosphors such as Y_2SiO_5:Ce^{3+} [13] and green oxide phosphors such as ZnO:Zn [14], $Y_3(Al, Ga)_5O_{12}$:Tb [13], Y_2SiO_5:Tb [13], which have a higher chemical stability, are potential blue and green luminescent materials for FEDs. The low efficiency and low color purity of these oxides, however, are a challenge for researchers to explore suitable blue and green phosphors with good chromaticity and high color purity. In this context, our efforts have been focused on the development of high color purity luminescent materials using the oxyapatite $Ca_2Gd_8Si_6O_{26}$ (CGS) host lattice by doping with trivalent rare-earth (RE^{3+}) ions.

The compounds with oxyapatite structure (space group $P6_3/m$) have been effective host lattices for luminescent materials due to their applications in solid-state lighting and FPD technologies. Among the many synthetic oxyapatites, the ternary rare-earth-metal silicate with the oxyapatite structure of the form

* Corresponding author. Tel.: +82 51 629 5569; fax: +82 51 629 5549.
E-mail address: bkmoon@pknu.ac.kr (B.K. Moon).

0925-8388/$ – see front matter © 2011 Elsevier B.V. All rights reserved.
doi:10.1016/j.jallcom.2011.04.122

$Ca_2RE_8Si_6O_{26}$ (RE = Y/Gd) is an efficient host lattice for the luminescence of various RE^{3+} activator ions and mercury like ions. This oxyapatite host lattice consists of two cationic sites, that is, the 9-fold coordinated 4f sites with C_3 point symmetry and 7-fold coordinated 6h sites with *Cs* point symmetry [15,16]. Both sites are suitable and can easily accommodate a great variety of RE^{3+} ions. Among the RE^{3+}, thulium or erbium doped phosphors have attracted substantial attention in recent years because Tm^{3+} and Er^{3+} ions provide blue and green emissions, respectively, with possible applications for the fabrication of FEDs [17,18].

The above applications demand single phase and compositionally uniform high purity powders with small and uniform particle size, for high resolution and high luminous efficiency. In view of this, solid-state reaction method [18] and several wet chemical techniques such as co-precipitation [19], sol–ge1 [10], combustion [20], hydrothermal [17], solvothermal [4] and spray-pyrolysis [21] have been explored to prepare the homogeneous phosphor precursor. These wet chemical processing methods offer an intimate mixing of starting materials and hence have shorter diffusion distances between reactants, thus requiring a relatively low temperature for the formation of final products with excellent chemical homogeneity [22]. However, to achieve high crystallinity and transform the powder into a dense ceramic, sintering at elevated temperatures becomes mandatory.

As far as we know, no information is available concerning the detailed photoluminescence (PL) and cathodoluminescence (CL) properties of Tm^{3+} or Er^{3+} doped CGS phosphors. Therefore, in this paper, we report the structural and detailed PL and CL properties of nanocrystalline CGS:Tm^{3+} and CGS:Er^{3+} phosphors prepared using solvothermal reaction method and sintered at 1200 °C for efficient blue and green emissions.

2. Experimental

Nanocrystalline CGS host lattices doped with Tm^{3+} or Er^{3+} were prepared by solvothermal process with the composition of $Ca_2(Gd_{1-x}Tm_x/Er_x)_8Si_6O_{26}$ (x = 0.5–6 mol%). The stoichiometric amounts of high purity grade calcium nitrate tetrahydrate ($Ca(NO_3)_2{\cdot}4H_2O$), gadolonium nitrate hexahydrate ($Gd(NO_3)_3{\cdot}6H_2O$), thulium nitrate pentahydrate ($Tm(NO_3)_3{\cdot}5H_2O$), erbium nitrate pentahydrate ($Er(NO_3)_3{\cdot}5H_2O$), and tetraethyl orthosilicate ($Si(OC_2H_5)_4$) were dissolved in 40 ml of 2-propanol. All reagents were taken without any further purification and stirred vigorously by using the magnetic stirrer until the formation of homogeneous solution and was transferred into a stainless steel autoclave with a Teflon liner (80 ml capacity and 50% filling). It was then heated to 230 °C at a rate of 2 °C/min and maintained for 5 h with magnetic stirring (at 180 rpm) to make stable networks between the reactants. After gradually cooling down to room temperature, the precipitate was separated by a centrifugal separator with 3000 rpm for 3 min and then dried at 50 °C for a day in the ambient atmosphere. The dried powder was sintered at different temperatures for 5 h and was brought to room temperature.

X-ray diffraction (XRD) patterns of sintered powders were recorded on *X' PERT-MPD* (*Philips, Netherlands*) X-ray diffractometer with CuKα = 1.5406 Å. The morphology of the sintered particles was examined by field emission scanning electron microscope (FE-SEM, *JEOL JSM-6700, Japan*). Osmium coating was sprayed on the sample surfaces using a fine coat ion sputter E-1010 unit (*Hitachi, Japan*) to avoid possible charging of specimens before SEM observation was made on each time. The room temperature PL spectra were recorded on a *Photon Technology International* (*PTI*, *USA*) fluorimeter with a Xe-arc lamp of power 60 W and the lifetimes were measured with a phosphorimeter attachment to the main system with a Xe-flash lamp (25 W power). The CL properties were measured by a *Gatan* (*UK*) *MonoCL3+* system attached with the SEM.

3. Results and discussion

Fig. 1 shows the representative XRD patterns of the pure CGS, CGS:Tm^{3+} and CGS:Er^{3+} phosphors sintered at 1200 °C. All the diffraction peaks are attributed to the hexagonal crystal form of oxyapatite based on the space group $P6_3/m$ and, which are in good agreement with the standard JCPDS card [PDF (28-0212)]. No impurity phase due to RE ions can be detected at the current doping level, indicating that the Tm^{3+} or Er^{3+} ions are completely dissolved into the Gd^{3+} sites of CGS host lattice. The full width at half maximum

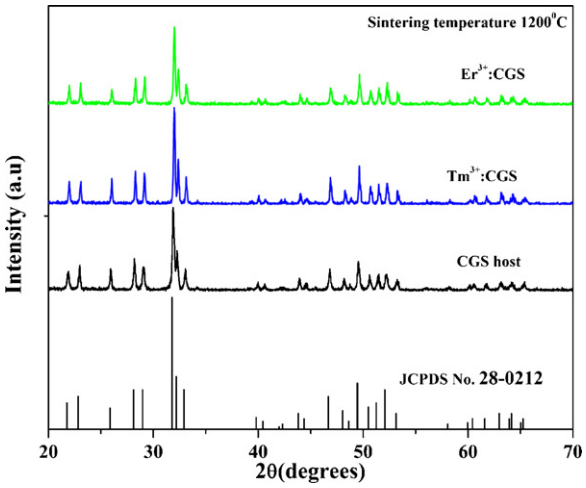

Fig. 1. XRD patterns of CGS host, CGS:Tm^{3+} and CGS:Er^{3+}.

(FWHM) of the strongest diffraction peaks are used to calculate the crystallite size by the Scherrer equation $D_{hkl} = k\lambda/\beta\cos\theta$, where D is the average grain size, k (0.9) is a shape factor, λ is X-ray wavelength (1.5406 Å), β is the FWHM and θ is the diffraction angle of an observed peak, respectively. The average values of about 48, 48, and 46 nm for pure CGS host, CGS:Tm^{3+}, and CGS:Er^{3+}, respectively. There is no considerable variation in the crystallite size because all the ions have nearly equal ionic radii Gd^{3+} (1 Å), Tm^{3+} (0.994 Å) and Er^{3+} (0.945 Å).

Fig. 2(a) and (b) shows the SEM images of obtained CGS:Tm^{3+}, and CGS:Er^{3+} phosphor samples sintered at 1200 °C. Both SEM images show almost the same morphology. The resulting particles have a spherical shape with sizes of around 100 nm due to the occurrence of agglomerations among the CGS particles during the period of sample sintering at 1200 °C. It is well known that the spherical-shaped particles are of greater importance because of their higher packing density, lower scattering of light and brighter luminescence performance.

Fig. 3(a) shows the photoluminescence excitation (PLE) spectrum of nanocrystalline CGS:Tm^{3+} phosphors by monitoring the emission wavelength at 456 nm. The spectrum shows a narrow excitation peak at 359 nm, which is assigned to the typical $4f^{12}$ intra-configurational $^3H_6 \rightarrow {}^1D_2$ transition and is the direct excitation of the Tm^{3+} ion from the ground state to $^1D_2$ excited level. The excitation peaks of Gd^{3+} between 250 and 320 nm have not considerable intensities, which indicate the very weak energy transfer between Gd^{3+} to Tm^{3+}.

It is known that the Tm^{3+} has complicated energy levels and different possible transitions because of the strong deviation from the Russell–Saunders coupling in the 4f configuration. Accordingly, the relaxation of highly excited states of the Tm^{3+} may take place via a large number of relaxation paths, resulting in ultra violet, visible, and infrared emissions with moderate intensity. Fig. 3(b) presents the room temperature visible PL spectrum of nanocrystalline CGS:Tm^{3+} phosphors under the excitation wavelength at 359 nm. Under UV irradiation, the emission color of CGS:Tm^{3+} phosphors appears bright blue to the naked eye, as shown in the inset of Fig. 3(b). The intense blue emission band observed at 456 nm, which corresponds to an electronic transition $^1D_2 \rightarrow {}^3F_4$. In addition to the intense $^1D_2$ manifold emission, very weak emissions were observed in the visible region at 475 nm due to $^1G_4 \rightarrow {}^3H_6$, and 516 nm due to $^1I_6 \rightarrow {}^3F_2$. Very weak intensity lines of the emission from the $^1G_4$ level could be the residual multiphonon non-radiative relaxation from $^1D_2$ level [23]. Note that, the 516 nm emission cannot be assigned to a $^1D_2 \rightarrow {}^3H_5$ transition because its intensity

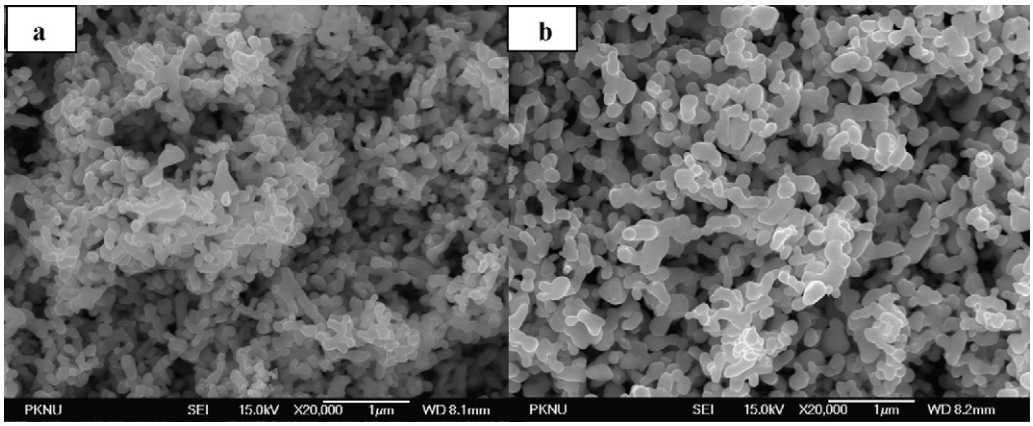

Fig. 2. SEM images of (a) CGS:Tm^{3+} and (b) CGS:Er^{3+}.

cannot behave as that of the 456 nm emission band. It probably originates from a higher lying Tm^{3+} energy level such as $^1I_6$ that we can locate approximately with other systems [24–26]. Interestingly, in CGS phosphors, the Tm^{3+} exhibits only strongest blue emission due to $^1D_2 \rightarrow {}^3F_4$ transition and other transition are very weak. Nakanishi et al. reported that the f–f transitions are forbidden by Laporte's selection rule, they are observed as a forced electric dipole transition when Tm occupies acentric sites as observed for Eu ion in Y_2O_3 [27]. In the same way in our CGS host lattice, the Tm^{3+} occupies acentric sites as observed for Eu^{3+} ion in CGS [28]. Some information on the crystal structure of hexagonal CGS is quite useful in explaining the dominant $^1D_2 \rightarrow {}^3F_4$ electric dipole transition. The CGS consists of two low symmetry cationic sites with C_3 and C_s point symmetries. Two Ca^{2+} and two Gd^{3+} ions are located at four 4f sites with C_3 point symmetry, and other six Gd^{3+} ions are distributed in six 6h site with C_s point symmetry. Both sites are very suitable for the luminescence of forced electric dipole transition for Tm^{3+} ions owing to their low symmetry features. When Tm^{3+} is doped in Gd^{3+}, because of its favorable size with Gd^{3+}, isomorphic substitution is easily possible and occupies simultaneously C_3 and C_s sites with equal probability in the lattice. Hence, the only electric dipole transition is possible, leading to the emission from electric dipole transitions. From this observation, it is also clear that the transition $^1I_6 \rightarrow {}^3F_2$ is appropriate at 516 nm.

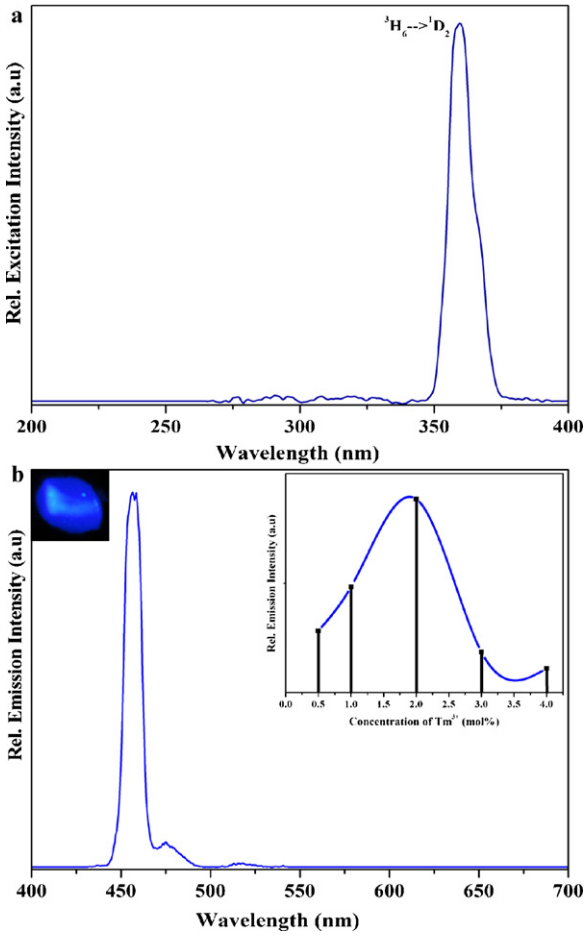

Fig. 3. (a) PLE spectrum of CGS:Tm^{3+} and (b) PL spectrum of CGS:Tm^{3+} (insets show the photograph of CGS:Tm^{3+} under UV irradiation and variation of the emission intensity as a function of Tm^{3+} concentration).

The inset of Fig. 3(b) shows the effect of Tm^{3+} concentration on the $^1D_2 \rightarrow {}^3F_4$ emission intensity. The emission intensity increases with increasing the Tm^{3+} concentration, reaching a maximum value at 2 mol%, and then decreases with further increasing the concentration of Tm^{3+}. This value is referred to as the optimum concentration of Tm^{3+} in CGS host lattice. It is noticeable that Tm^{3+}-activated phosphors show relatively low activator concentration compared with Eu^{3+} and Tb^{3+} activated phosphors in the same host at about 6 mol% [28,29]. This is ascribed to the enhanced strength of the dipolar interaction between the neighboring activator ions [30,31].

Fig. 4(a) shows the excitation spectrum of nanocrystalline CGS:Er^{3+} phosphors by monitoring the emission wavelength at 550 nm. The spectrum consists of intra 4f-transitions of Er^{3+} transitions in the longer wavelength region from the ground state $^4I_{15/2}$ to the excited states $^2G_{7/2}$, $^4G_{9/2}$, $^4G_{11/2}$, $^2H_{9/2}$, $^4F_{3/2}$, $^4F_{5/2}$, and $^4F_{7/2}$ at 358, 367,380, 409, 443, 453, and 489 nm, respectively. The excitation spectrum also contains the weak Gd^{3+} intra 4f transitions in the shorter wavelength region at 276, 308, and 314 nm due to the electronic transitions $^8S_{7/2} \rightarrow {}^6I_{11/2}$, $^8S_{7/2} \rightarrow {}^6P_{7/2}$, and $^8S_{7/2} \rightarrow {}^6P_{7/2}$, respectively. This means that the energy transfer from Gd^{3+} to Er^{3+} in the CGS host lattice is not efficient. Among the Gd^{3+} and Er^{3+} excitation peaks, the excitation peak at 380 nm due to $^4I_{15/2} \rightarrow {}^4G_{11/2}$ was dominated.

Fig. 4(b) presents the visible emission spectrum of nanocrystalline CGS:Er^{3+} phosphors by excitation at 380 nm ($^4I_{15/2} \rightarrow {}^4G_{11/2}$) wavelength, which is attributed to the transitions in the $4f^{11}$ shell. Under UV irradiation, the emission color of CGS:Er^{3+} phosphors is strong green to the naked eye, as shown in the inset of Fig. 4(b). The spectrum exhibits two emission bands due to $^2H_{11/2} \rightarrow {}^4I_{15/2}$ and $^4S_{3/2} \rightarrow {}^4I_{15/2}$ transitions at 528 and 550 nm, respectively in the green region. Note that the red emission due to $^4F_{9/2} \rightarrow {}^4I_{15/2}$

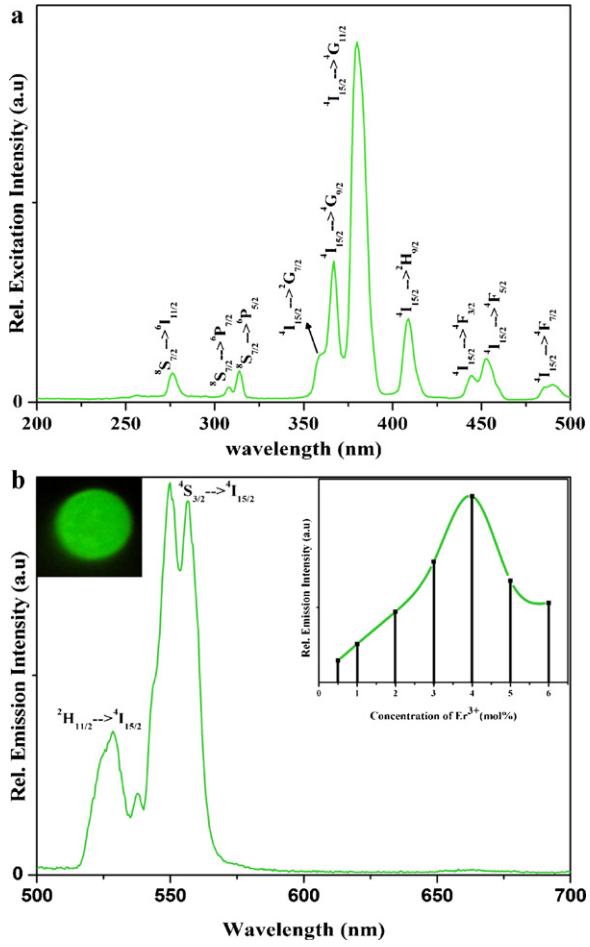

Fig. 4. (a) PLE spectrum of CGS:Er^{3+} and (b) PL spectrum of CGS:Er^{3+} (inset shows the photograph of CGS:Er^{3+} under UV irradiation and variation of the emission intensity as a function of Er^{3+} concentration).

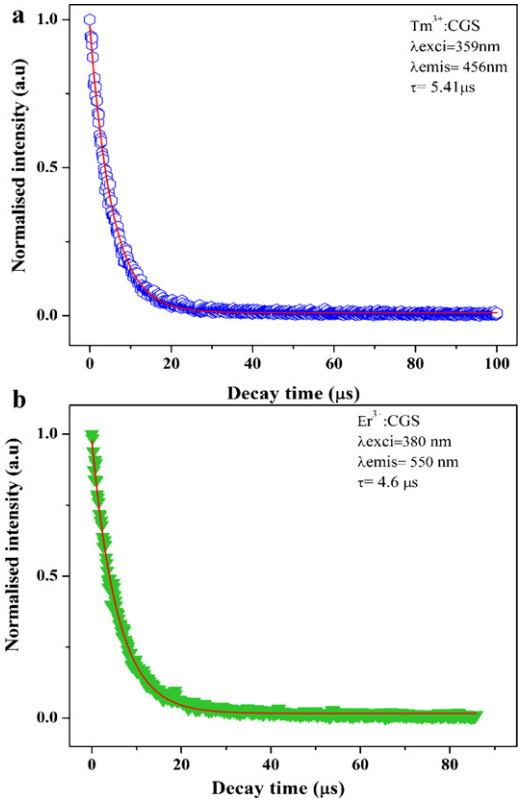

Fig. 5. Decay curves of the (a) CGS:Tm^{3+} and (b) CGS:Er^{3+}.

at 650 nm was not observed, indicating that a very efficient non-radiative relaxation for the $^4F_{9/2}$ level occurred. Generally, in inorganic phosphors, the visible emission of Er^{3+} in only the green region is very rare [32,33]. From the spectrum it is clear that the emission peaks of Er^{3+} were centered in the green region only, so its color coordinates are precious. The inset of Fig. 4(b) shows the effect of Er^{3+} concentration on the green emission intensity. There was no effect of concentration on the spectral shape of Er^{3+} in the CGS host lattice. The green emission intensity increases with increasing the Er^{3+} concentration upto 4 mol%, and then decreases with further increasing the concentration of Er^{3+}. This value is referred to as the optimum concentration of Er^{3+} in CGS host lattice. The Er^{3+} ions in the low concentration are usually randomly distributed in the host lattice and Er^{3+}–Er^{3+} distances are too far apart, but at the higher concentration the distance between the two Er^{3+} ions are reduced, thus leading to the formation of Er^{3+} clusters. As a result, concentration quenching process will be occurred at a higher concentration.

Blasse assumed that for the critical concentration the average shortest distance between the nearest activator ions is equal to the critical distance [34]. Therefore, the critical distance (R_c) for Tm^{3+} and Er^{3+} in the CGS host lattice can be estimated by the following equation;

$$R_c \approx 2\left(\frac{3V}{4\pi x_c N}\right)^{1/3}$$

where V is the volume of the unit cell, x_c is the critical concentration and N is the number of cationic sites in the unit cell. In the present work, V is 518.099 $Å^3$, N is 8, x_c is about 0.02, and 0.04 for Tm^{3+} and Er^{3+}, respectively. The calculated R_c was about 18.36 Å for Tm^{3+} and 14.57 Å for Er^{3+}.

The decay profiles of the $^1D_2 \rightarrow {}^3F_4$ emission level of CGS:Tm^{3+} and $^4S_{3/2} \rightarrow {}^4I_{15/2}$ emission level of CGS:Er^{3+}nanocrystalline phosphors at the optimized concentrations are presented in Fig. 5(a) and (b). The results demonstrated that the decay profiles of both the samples were well fitted to single exponential, $I = I_0 \exp(-t/\tau)$, where τ is the decay time. From these profiles, the lifetimes of Tm^{3+} and Er^{3+} were determined to be 5.41 μs and 4.6 μs, respectively.

Fig. 6(a) and (b) shows the low voltage (3 kV) CL properties of nanocrystalline CGS:Tm^{3+} and CGS:Er^{3+} phosphors, respectively. From Fig. 6(a) it is clear that, under the low voltage electron beam excitation, for CGS:Tm^{3+} phosphors, the CL properties are slightly different from the PL properties. The CL spectrum of CGS:Tm^{3+} exhibits strong blue luminescence corresponding to the electronic transitions $^1D_2 \rightarrow {}^3F_4$ at 459 nm and $^1G_4 \rightarrow {}^3H_6$ at 476 nm, and the transition $^1I_6 \rightarrow {}^3F_2$ in the green region has not been observed. This spectral quality confirms high color purity and excellent chromaticity coordinates in the blue region. For CGS:Er^{3+} phosphors, the CL spectral properties are similar to their PL spectra as shown in Fig. 6(b). Under the low voltage electron beam excitation, the CGS:Er^{3+} shows only the strong green lines associated with the erbium intraionic transitions $^2H_{11/2} \rightarrow {}^4I_{15/2}$ at 527 nm and $^4S_{3/2} \rightarrow {}^4I_{15/2}$ at 556 nm.

The CL emission intensities of CGS:Tm^{3+} and CGS:Er^{3+} phosphors were obtained as a function of accelerating voltage. When the filament current is fixed at 108 μA, the CL intensity increases in both CGS:Tm^{3+} and CGS:Er^{3+} phosphors with increasing the accelerating voltage from 1 kV to 5 kV as showed in the inset of Fig. 6(a) and (b). The intensity enhancement with accelerating voltage is ascribed to the increase in the penetration depth of electrons in the

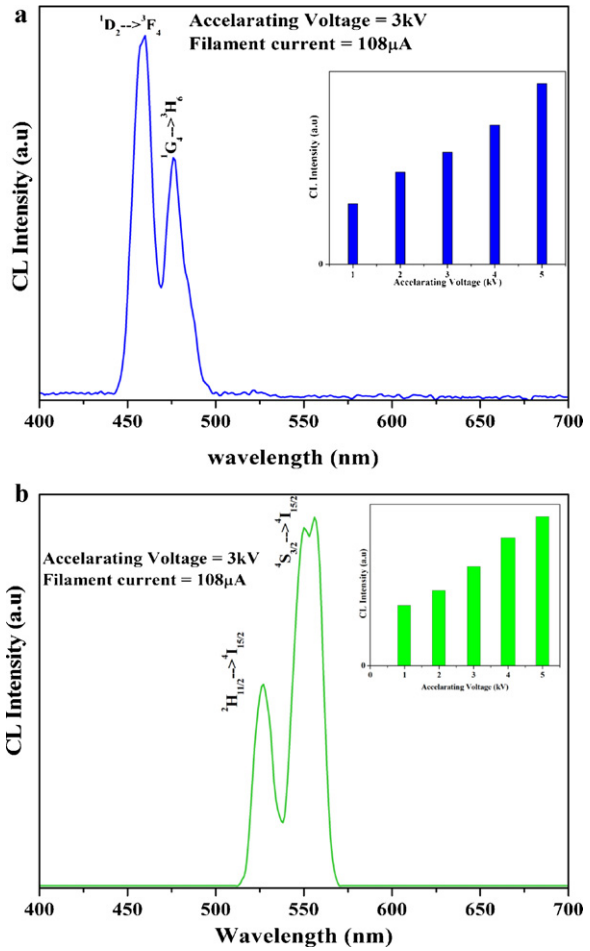

Fig. 6. CL spectra of (a) CGS:Tm^{3+} and (b) CGS:Er^{3+} (insets show the variation of the emission intensity as a function of accelerating voltage)

sample. At high accelerating voltage, more plasma is produced by incident electrons, which excites more Er^{3+} and Tm^{3+} ions. The penetration of the electron beam into a particular sample is affected by the energy of the electron beam. For higher electron beam energy, the penetration depth becomes larger [2].

According to the European Broadcasting Union (EBU) and National Television System Committee (NTSC) standards, the basic requirements for display phosphors are stability and emission color purity. The color purity can be calculated by the following equation [35];

$$\text{Color purity} = \frac{\sqrt{(x-x_i)^2+(y-y_i)^2}}{\sqrt{(x_d-x_i)^2+(y_d-y_i)^2}}$$

where (x, y) and (x_i, y_i) are the color coordinates of the light source and the CIE illuminant, respectively, and (x_d, y_d) color coordinates of the dominant wavelength. The dominant wavelength is determined by drawing a straight line from the illuminant C to the (x, y) coordinates of our samples, and by extending the straight line to the perimeter of the chromaticity diagram. The intersection point is the dominant wavelength of light source. The chromaticity coordinates, and color purity compared to the 1931 CIE standard source C (0.3101, 0.3162) for CGS:Tm^{3+} and CGS:Er^{3+} phosphors were determined from the PL and CL spectra.

Fig. 7 shows the CIE color coordinates calculated from PL spectra of nanocrystalline CGS:Tm^{3+} and CGS:Er^{3+} phosphors in comparison with some important commercial phosphors. For the CGS:Tm^{3+} phosphors, the CIE coordinates are determined to be (0.165, 0.064)

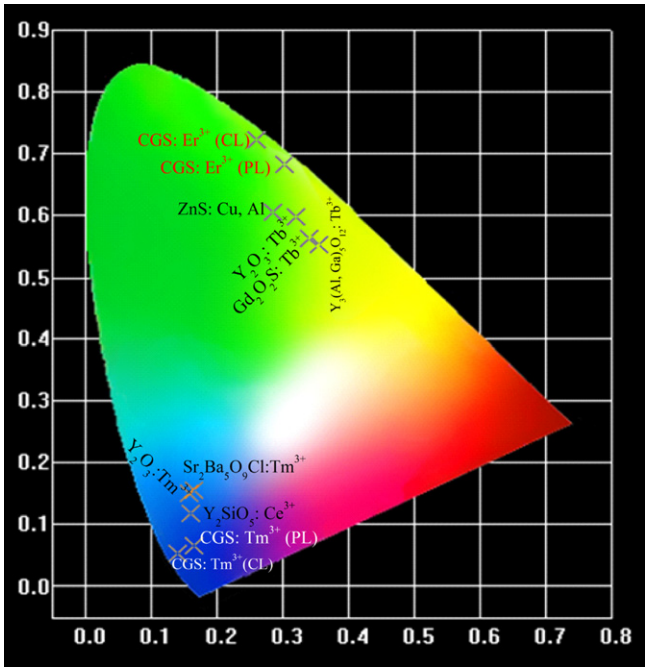

Fig. 7. CIE chromaticity diagram for CGS:Tm^{3+} and CGS:Er^{3+} and some important commercial phosphors

with a color purity of 87%, which is identical to the EBU illuminant blue (0.15, 0.0651) and also NTSC illuminant blue (0.14, 0.08). The obtained blue (x, y) coordinates are very close to the commercially available blue phosphors, such as Y_2O_3:Tm (0.158, 0.150) [21], $Sr_2B_5O_9Cl$:Tm (0.166, 0.155) [36], and $ZnGa_2O_4$ (0.175, 0.186) [13]. The calculated CIE coordinates of nanocrystalline CGS:Er^{3+} phosphors are (0.303, 0.683) with 96% color purity, which is superior to the commercially available green phosphors, such as Y_2O_3:Tb^{3+} (0.319, 0.597) [21], ZnS:Cu, Al (0.284, 0.605) [37], and $SrGa_2S$:Eu^{2+} (0.32, 0.63) [11]. The obtained green (x, y) coordinates are also very close to the EBU green (0.29, 0.60) and NTSC green (0.21, 0.71).

The CIE color coordinates calculated from CL spectra of nanocrystalline CGS:Tm^{3+} and CGS:Er^{3+} phosphors are also shown in Fig. 7. The obtained blue (x, y) chromaticity coordinates are (0.141, 0.0523) with a color purity of 95%, which is superior to those commercially available FED phosphors Y_2SiO_5:Ce^{3+} (0.159, 0.118) [13] and ZnS:Ag (0.150, 0.052) [12]. The green chromaticity coordinates are determined to be (0.259, 0.723) with a color purity of 96%, which is better quality to those reported currently available commercial green FED phosphors, such as ZnO:Zn (0.25, 0.44) [14], Gd_2O_2S:Tb^{3+} (0.341, 0.562) [11], $Y_3(Al, Ga)_5O_{12}$:Tb (0.354, 0.553) [13] and Y_2SiO_5:Tb (0.333, 0.582) [13]. Phosphors with such superior color quality emit primarily blue and green light, from which a wide spectrum of colors is generated by appropriate mixing.

4. Conclusions

Nanocrystalline CGS:Tm^{3+} and CGS:Er^{3+} phosphors were successfully prepared by solvothermal reaction method. XRD patterns confirmed their hexagonal structure and SEM measurements showed the spherical morphology. The PL spectra of CGS:Tm^{3+} under 359 nm excitation and CGS:Er^{3+} under 380 nm excitation exhibited the strong blue ($^1D_2 \rightarrow {}^3F_4$ at 456 nm) and green ($^4S_{3/2} \rightarrow {}^4I_{15/2}$ at 550 nm) colors with the color purity 87% and 96%, respectively. The low accelerating voltage CL spectra of CGS:Tm^{3+} and CGS:Er^{3+} also led to the strong blue and green emissions with the color purity 95% and 96%, respectively. On the basis of the results obtained in the present work, we could suggest these phosphors

could consider as novel luminescent materials in the blue and green regions for LEDs and FED devices.

Acknowledgements

This research was supported by NCRC (National Core Research Center) program through the National Research Foundation of Korea funded by the Ministry of Education, Science and Technology (2010-0001-226).

References

[1] S. Ye, F. Xiao, Y.X. Pan, Y.Y. Ma, Q.Y. Zhang, Mater. Sci. Eng., R 71 (2010) 1–34.
[2] G. Li, Z. Hou, C. Peng, W. Wang, Z. Cheng, C. Li, H. Lian, J. Lin, Adv. Funct. Mater. 20 (2010) 3446–3456.
[3] B. Dierre, X. Yuan, T. Sekiguchi, Sci. Technol. Adv. Mater. 11 (2010) 043001.
[4] Y. Tian, B. Chen, B. Tian, R. Hua, J. Sun, L. Cheng, H. Zhong, X. Li, J. Zhong, Y. Zheng, T. Yu, L. Huang, Q. Meng, J. Alloys Compd. 509 (2011) 6096–6101.
[5] H.A. Höppe, Angew. Chem. Int. Ed. 48 (2009) 3572–3582.
[6] S.-A. Yan, Y.-S. Chang, W.-S. Hwang, Y.-H. Chang, M. Yoshimura, C.-S. Hwang, J. Alloys Compd. 509 (2011) 5777–5782.
[7] H.L. Li, H.L.W. Chan, J.H. Hao, J. Phys. D: Appl. Phys. 42 (2009) 185103.
[8] N. Hirosaki, R.-J. Xie, K. Inoue, T. Sekiguchi, B. Dierre, K. Tamura, Appl. Phys. Lett. 91 (2007) 061101.
[9] P. Psuja, D. Hreniak, W. Strek, Nanomater. J. 2007 (2007) 81350.
[10] T. Nagase, H. Kominami, Y. Nakanishi, K. Shinozaki, N. Mizutani, Thin Solid Films 518 (2010) 3875–3878.
[11] S. Yang, C. Stoffers, F. Zhang, S.M. Jacobsen, B.K. Wagner, C.J. Summers, Neil. Yocom, Appl. Phys. Lett. 72 (2) (1998) 158–160.
[12] R.Y. Lee, S.W. Kim, J. Lumin. 93 (2001) 93–100.
[13] T. Jüstel, H. Nikol, C. Ronda, Angew. Chem. Int. Ed. 37 (1998) 3084–3103.
[14] M. Leskelä, J. Alloys Compd. 275–277 (1998) 702–708.
[15] G. Blasse, J. Solid State Chem. 14 (1975) 181–184.
[16] M.D. Chambers, P.A. Rousseve, D.R. Clarke, J. Lumin. 129 (2009) 263–269.
[17] J. Liao, B. Qiu, H. Wen, J. Chen, W. You, L. Liu, J. Alloys Compd. 487 (2009) 758–762.
[18] F. Zhang, Y. Wang, J. Liu, J. Alloys Compd. 509 (2011) 3852–3854.
[19] Y. Dong, Z. Wu, X. Han, R. Chen, W. Gu, J. Alloys Compd. 509 (2011) 3638–3643.
[20] H. Erdem Çamurlu, J. Alloys Compd. 509 (2011) 5431–5436.
[21] J. Hao, S.A. Studenikin, M. Cocivera, J. Lumin. 93 (2001) 313–319.
[22] O. Yamaguchi, K. Takeoka, K. Hirota, H. Takano, A. Hayashida, J. Mater. Sci. 27 (1992) 1261–1264.
[23] L. Macalik, J. Hanuza, D. Jaque, J. García Solé, Opt. Mater. 28 (2006) 980–987.
[24] G.H. Dieke, Spectra and Energy Levels of Rare Earth Ions in Crystals, Wiley Interscience, New York, 1968.
[25] C. Li, A. Lagriffoul, R. Moncorge, J.C. Souriau, C. Borel, Ch. Wyon, J. Lumin. 62 (1994) 157–171.
[26] J. Sanz, R. Cases, R. Alcala, J. Non-Cryst. Solids 93 (1987) 377–386.
[27] Y. Nakanishi, H. Wada, H. Kominami, M. Kottaisamy, T. Aoki, Y. Hatanaka, J. Electrochem. Soc. 146 (11) (1999) 4320–4323.
[28] G. Seeta Rama Raju, H.C. Jung, J.Y. Park, B.K. Moon, R. Balakrishnaiah, J.H. Jeong, J.H. Kim, Sens. Actuators B 146 (2010) 395–402.
[29] G. Seeta Rama Raju, H.C. Jung, J.Y. Park, B.K. Moon, J.H. Jeong, J.H. Kim, J. Electrochem. Soc. 158 (2) (2011) J20–J26.
[30] B. Yan, X.-Q. Su, Opt. Mater. 29 (2007) 1866–1870.
[31] O.A. Lopez, J. McKittrick, L.E. Shea, J. Lumin. 71 (1997) 1–11.
[32] Y.-C. Li, Y.-H. Chang, Y.-F. Lin, Y.-J. Lin, Y.-S. Chang, Appl. Phys. Lett. 89 (2006) 081110.
[33] F. Vetrone, J.-C. Boyer, J.A. Capobianco, A. speghini, M. Bettinelli, Chem. Mater. 15 (14) (2003) 2737–2743.
[34] G. Blasse, Philips Res. Rep. 24 (1969) 131–144.
[35] E. Fred Schubert, Light Emitting Diodes, 2nd ed., Cambridge University Press, 2006, pp. 300–301, chapter 17.
[36] J. Hao, M. Cocivera, J. Phys.: Condens. Matter 14 (2002) 925–933.
[37] C-H. Chang, B-S. Chiou, K-S. Chen, C-C. Ho, J.-C. Ho, Ceram. Int. 31 (2005) 635–640.